

Correlated percolation in island-forming processes: Analysis of cooperative filling on a square lattice

D. E. Sanders and J. W. Evans

Ames Laboratory and Department of Chemistry, Iowa State University, Ames, Iowa 50011

(Received 12 February 1988)

Percolation transitions are analyzed for correlated distributions of occupied sites created by irreversible cooperative filling on a square lattice. Filling can be either autocatalytic, corresponding to island formation, or autoinhibitory. Here percolation problems for occupied and unoccupied clusters are generally distinct. Our discussion focuses on the influence of island formation (associated with correlation lengths of many lattice vectors), and of island perimeter roughness, on percolation. We also discuss the transition to continuum percolation problems as the ratio of island growth to nucleation rates, and thus the average island size, diverges. Some direct analysis of occupied cluster structure is provided, the connection with correlated animals is made, and correlated spreading and walking algorithms are suggested for direct generation of clusters and their perimeters.

I. INTRODUCTION

The random-site-percolation problem¹ provides a simple example of a geometric critical phenomenon. Here one randomly occupies a certain fraction p of sites on an infinite lattice, introduces a connectivity rule to define clusters of occupied sites, and then examines the properties of these clusters. Of primary interest is the behavior near the critical occupancy p_c where a cluster of occupied sites first spans the lattice or "percolates." Clearly the (random) statistics of the unoccupied sites (o), for occupancy $1-p$, are equivalent to those of the occupied sites (x), for occupancy p . Consequently, the percolation problem for clusters of unoccupied sites (defined by the same connectivity rule) is not distinct here, and the associated critical occupancy, p'_c , equals $1-p_c$.

The concepts and techniques associated with this problem have also played a central role in the description of disordered systems.² However, it is clear that randomness is an idealization for physical systems where correlations typically exist. Consequently several studies have considered percolation in correlated systems.³ Most commonly, the correlations were prescribed by an Ising or Potts model, in part because such models are so well characterized, and in part to study the connection between thermal and geometric critical phenomena. For the latter, it has become clear that a judicious choice of connectivity rule is required.⁴ However, such an imposition of "equilibrium" statistics is somewhat restrictive. For example, in the Ising model with pairwise additive interactions, percolation problems for occupied and unoccupied sites are still equivalent. Physical systems often exist in unequilibrated or metastable states, and exhibit no such symmetries. There have been only a few corresponding percolation studies utilizing, e.g., restricted valence⁵ or Voter models,⁶ and a more generic study for Bethe lattices.⁷

Here we study the percolative aspects of a class of nonequilibrium distributions generated by irreversible cooperative filling of the sites on a lattice.⁸ These models

are described in detail below. Of particular interest here are such models which incorporate an island-forming propensity, and thus can exhibit correlation lengths ξ_0 of many times the lattice constant a . The following general questions are of interest. What is the effect of island formation, and, e.g., island perimeter roughness,⁹ on the percolative properties? How does the correlation length ξ_0 relate to the connectivity length ξ ? (The latter gives the average separation between two occupied sites in the same cluster.) If one thinks of these processes as involving the essentially random linkage of "individual" islands to form ramified clusters of these, then one expects to find random percolation behavior on a large length scale (ξ_0 replaces a as the "unit" of length). We are also interested in relating such lattice island-growth models, as $\xi_0 \rightarrow \infty$, to continuum grain growth type models, and relating the associated lattice and continuum percolation problems.

A mathematical formulation of the behavior of such systems near the percolation transition, exploiting random percolation concepts, is given below. Here we assume that *individual* islands (before coalescence) are compact consisting of $s_0 = O(\xi_0^2)$ occupied sites. Let n_s (R_s) denote the average number (radius of gyration) of clusters of s occupied sites. Let $s_{av} = \sum_s s^2 n_s / \sum_s s n_s$ (s_{dom}) denote the average (dominant) number of occupied sites per cluster. Let p denote the fraction of occupied sites, and p_c its value at the occupied site percolation threshold. Then one expects that for p near p_c (cf. Ref. 1),

$$\begin{aligned} \xi/\xi_0 &\sim |p-p_c|^{-\nu}, \\ s_{av}/s_0 &\sim |p-p_c|^{-\gamma}, \\ s_{dom}/s_0 &\sim |p-p_c|^{-1/\sigma}, \\ s_0 n_s &\sim (s/s_0)^{-\tau} f((p-p_c)(s/s_0)^\sigma), \end{aligned} \quad (1)$$

where f is a scaling function, and the critical exponents ν , γ , τ , and σ satisfy $\gamma = (3-\tau)/\sigma$, $2\nu = (\tau-1)/\sigma$. We are also interested in the behavior of the effective dimension of occupied clusters \bar{d} (for lengths many times ξ_0). If \bar{d} is defined by $s_{dom}/s_0 \sim (\xi/\xi_0)^{\bar{d}}$, then from (1),

$\bar{d} = (\sigma v)^{-1}$ at p_c . This is also true using $R_s/\xi_0 \sim (s/s_0)^{1/\bar{d}}$ to determine \bar{d} , as can be established by equating critical exponents for both sides of the identity $\xi^2 = 2 \sum_s R_s^2 s^2 n_s / \sum_s s^2 n_s$.¹ Random percolation studies suggest that \bar{d} , determined from R_s behavior for large finite s , will increase with p . From comments above, we expect that the critical exponents will assume their random percolation values for all these models with finite ξ_0 . However, p_c will be model dependent.

In general, the statistics of occupied sites, for occupancy p , and unoccupied sites, for occupancy $1-p$, will be distinct. Thus one must independently consider the percolative characteristics of unoccupied clusters, noting that the associated critical occupancy p'_c will not, in general, equal $1-p_c$. A mathematical development analogous to (1) can be given, and again we expect random percolation critical exponents. Here we consider only two-dimensional problems with a choice of connectivity rule for which occupied and unoccupied clusters *cannot* cross. Then topological arguments imply that they cannot simultaneously percolate,¹⁰ and thus that $p'_c \leq p_c$.

Cluster perimeter structure is also of interest. A scaling theory for the external perimeters or "cluster hulls," together with the internal perimeters, can be developed analogous to that for the clusters themselves.¹¹ Universality questions pertaining to such hull structure have received little attention. Does the effective dimension of the hull (for lengths many times ξ_0) equal the random percolation value of $\frac{7}{4}$ at p_c ? Here we shall make only a few comments on hull structure. However, we shall also consider the behavior of the total number t of unoccupied sites "adjacent" to external and internal occupied cluster perimeter sites. As the occupied cluster size s diverges, t/s should approach a nonzero limit¹ of at least $O(\xi_0^{-1})$, depending on perimeter roughness.

The two-dimensional lattice studies presented here have relevance to the geometric characterization of surface adlayer structure in the submonolayer regime.¹² In particular, we mention the case for island-forming chemisorption processes, which involve competition between nucleation, growth and coalescence of islands.¹³ A primary objective of surface-sensitive diffraction studies is to determine an "average island size" from beam half-widths. For adlayer states consisting of regular well-separated islands, this size measure is unambiguous. However for percolative structures, the measure obtained from diffraction will not in general correspond to any island size measure which diverges at p_c .¹⁴ The structure of adsorbate islands or clusters will influence: the nature of equilibration and adlayer phase transitions,¹⁵ the kinetics of adsorbate-induced reconstruction,¹⁶ and nonequilibrium desorption kinetics.¹⁷ Vibrational excitations associated with the adlayer¹⁸ must be localized below a suitably defined percolation threshold. More complicated surface processes, involving coadsorption and subsequent reaction of various species, have also been shown to produce fractal islands in the random percolation universality class,¹⁹ as with the models discussed here. Finally we note that the concepts developed here should be particularly useful in characterizing surface structure in layer-by-layer epitaxial growth processes.²⁰

In Sec. II we describe in detail the irreversible cooperative filling model. We analyze the scaling behavior of the correlation length as the ratio of island growth to nucleation rates increases, as well as the structure of individual growing islands, for two classes of rate choice. Some direct analysis of occupied cluster structure is also given. A finite-size scaling analysis of the percolation transitions in these models is provided in Sec. III. A preliminary account of these results was provided in Ref. 12. The effect of island perimeter roughness on percolation thresholds is considered in Sec. IV. In Sec. V, correlated spreading and walking algorithms are described for the direct generation of individual percolation clusters, and their connected perimeters, respectively. Finally we summarize our findings, and suggest various extensions to this work in Sec. VI.

II. IRREVERSIBLE COOPERATIVE FILLING ON A SQUARE LATTICE

In these models, sites on an infinite square lattice are filled irreversibly with rates k_j depending on the number j of occupied nearest-neighbor (NN) sites.⁸ We describe filling as autoinhibitory if k_0 is larger than the other rates, and autocatalytic if it is smaller. In the latter case, island formation occurs, the rate k_0 being associated with island nucleation, $k_1 = \alpha k_0$ ($\alpha > 1$) with growth, and k_2 , k_3 , and k_4 with growth or coalescence. Clearly as α increases, so will various measures of average island size, and $\alpha \rightarrow \infty$ will correspond to a "continuum limit." In this analysis, we define occupied (unoccupied) clusters as sets of occupied (unoccupied) sites connected by NN bonds. Note that occupied and unoccupied clusters cannot cross for this choice of short-range connectivity (in contrast to longer-range choices), so $p'_c \leq p_c$. We have previously described a shielding property satisfied by unoccupied (but *not* occupied) sites,⁸ which indicates the lack of symmetry between the statistics of unoccupied and occupied sites.

The scaling exponent ω of the characteristic or correlation length, $\xi_0 \sim c\alpha^\omega$, as $\alpha \rightarrow \infty$, and the structure of individual growing islands depends on the form of k_j/k_0 as functions of α . Let C_l denote the pair-correlation function for sites separated by l lattice vectors, and let n_s denote the number of clusters of s occupied sites (as previously). Then for large α , these quantities should assume the scaling forms

$$C_l \sim C[l/\xi_0, \Theta] \text{ and } s_0 n_s \sim N[s/s_0, \Theta]. \quad (2)$$

Here $s_0 = O(\xi_0^2)$ since individual islands in these models are compact, and the functions $C[]$ and $N[]$ will depend on the choice of k_j/k_0 . Let m_s denote the number of horizontal or vertical strings of exactly s consecutive occupied sites. Then to analyze scaling behavior, it will be useful to consider the averages $m_{av}(i) = \sum_s s^i m_s / \sum_s s^{i-1} m_s$. Let D denote the probability of a NN empty-filled pair. Then note that $m_{av}(1) = \Theta/D$ is a local quantity, and is thus readily determined.⁸ We shall see that m_s does *not* always have a large- α scaling form, $\xi_0 m_s \sim M[s/\xi_0, \Theta]$ (at least for the α ranges considered here). However, when such scaling holds, it implies that

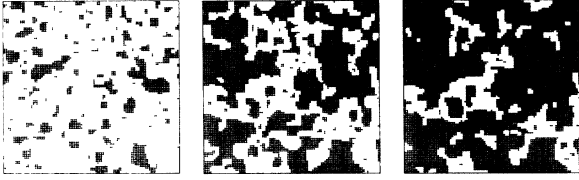


FIG. 1. Filling with multiplicative rates for $\alpha=19$: typical occupied site distributions for $p=0.2, 0.6$ (near p_c), and 0.8 .

$$m_{\text{av}}(i) \sim \xi_0 \int dy y^{i+1} M[y, \Theta] / \int dy y^i M[y, \Theta].$$

Similar remarks apply for diagonal strings of occupied sites.

In addition to large- α scaling behavior, we are interested in the coverage dependence of various quantities (for fixed α). These include the effective dimension \bar{d} of occupied clusters, and the $s \rightarrow \infty$ limit of the total perimeter length (t) to island size (s) ratio. Here t denotes the number of unoccupied sites NN to the (perimeter) sites of a cluster of s occupied sites. In the $p \rightarrow 0$ limit, these quantities describe the behavior of suitably *correlated animals*. The weight associated with any such animal $\{s\}$ of s occupied sites, is determined by the lead coefficient $c_{\{s\}}$ in the formal expansion, $c_{\{s\}} p^s + O(p^{s+1})$, for the probability of the cluster $\{s\}$. For these filling models, $(k_0)^s c_{\{s\}}$ is simply given by the average of products of rates associated with each of the $s!$ orders of filling sites in $\{s\}$.²¹

A. Multiplicative rates: $k_j \propto \alpha^j$

For $\alpha \gg 1$, individual islands tend to be rectangular for linear sizes up to $O(\alpha^{1/2})$: addition to the edge of a per-

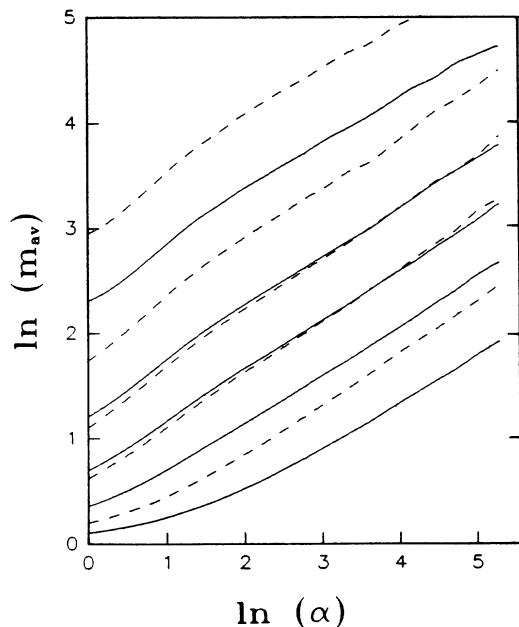


FIG. 2. Scaling of $m_{\text{av}}(i)$ with α for multiplicative rates. Solid (dashed) lines correspond to $i=1$ ($i=2$) for $p=0.1, 0.3, 0.5, 0.7$, and 0.9 (from bottom to top). Large- α slopes, $(d/d \ln \alpha) \ln m_{\text{av}}(i)$, are close to $\frac{1}{2}$.

TABLE I. The reciprocal effective dimension $\rho = 1/\bar{d}$ for occupied clusters generated by filling with multiplicative rates. Values for various α and $p/p_c(\alpha)$ are shown.

α	$\frac{1}{2}$	$\frac{p/p_c}{\frac{5}{6}}$	1
$\frac{1}{2}$		0.65	0.56
1	0.65	0.58	0.54
2	0.61	0.58	0.54
4	0.61	0.60	0.56
9	0.64	0.59	0.55

fect rectangle with rate k_1 is rate determining; addition is then quickly completed by filling along this kinked edge with much larger rate k_2 .⁸ When two islands meet, they rapidly expand (via filling with rate k_2) to form a larger rectangular island encompassing both. Figure 1 shows occupied site distribution for various p values for a simulated lattice filling with $\alpha=19$.

Previous analyses have shown that the correlation length satisfies $\xi_0 \sim c \alpha^\omega$, with $\omega = \frac{1}{2}$.^{8,22} For this process, the growing clusters contain very few defects or holes. Said differently, the cluster growing or active zone has a width $O(1)$. This implies that the quantities $m_{\text{av}}(i)$ should also scale like ξ_0 or $\alpha^{1/2}$, for large α . This behavior is confirmed by simulation results for $m_{\text{av}}(1)$ and $m_{\text{av}}(2)$, which must be asymptotically proportional (see Fig. 2).

Next we consider the variation, with p and α , of the effective dimension, $\bar{d} \equiv 1/\rho$, and the total perimeter length to size ratio t/s for large occupied clusters. Data was obtained from 20 simulated fillings on a 200×200 site lattice with periodic-boundary conditions. Thus our statistical errors are large, particularly for smaller p where our statistical sample contains insufficient large clusters. Table I shows ρ values obtained from the slope of $\ln R_s$ versus $\ln s$ plots for $s \geq 15$. These ρ values consistently decrease with increasing p (corresponding to increasing \bar{d}). Significant statistical errors are apparent in the $\alpha=1$ value for $p/p_c = \frac{1}{2}$ which has already exceeded the $p=0$ random animal upper bound of 0.64. However, these results suggest that ρ always achieves the random percolation universal value of 0.53 at the α -dependent p_c (determined in Sec. III). Table II shows values for $\lim_{s \rightarrow \infty} t/s$. Our $\alpha=1$ random percolation values agree with previous accurate estimates for $p/p_c=1$ and $\frac{5}{6}$.

TABLE II. $\lim_{s \rightarrow \infty} t/s$ for occupied clusters generated by filling with multiplicative rates. Values for various α and $p/p_c(\alpha)$ are shown.

α	$\frac{1}{2}$	$\frac{p/p_c}{\frac{5}{6}}$	1
$\frac{1}{2}$	1.34	0.94	0.62
1	1.23	0.89	0.69
2	0.97	0.78	0.65
4	0.70	0.59	0.50
9	0.53	0.40	0.34
19	0.35	0.27	0.22

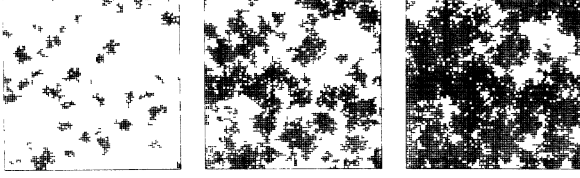


FIG. 3. Filling with Eden rates for $\alpha=499$: typical occupied site distributions for $p=0.15, 0.5$ (near p_c), and 0.75 .

However, the $p/p_c = \frac{1}{2}$ value is too high (by 0.2). Corresponding errors are expected for other α values. Note that $\lim_{s \rightarrow \infty} t/s$ tends to decrease with increasing clustering propensity $\alpha \geq 1$. Similar behavior occurs for distributions with two-dimensional Ising-model correlations.²³ The unusual decrease in $\lim_{s \rightarrow \infty} t/s$ at p_c , as α is lowered from 1 to $\frac{1}{2}$, also mimics near p_c Ising-model behavior.²³ We expect that $\lim_{s \rightarrow \infty} t/s$ scales like ξ_0^{-1} or $\alpha^{-1/2}$, for large α . Behavior of these quantities when $p \rightarrow 0$ is associated with correlated animals $\{s\}$, with weights $c_{\{s\}} = \alpha^{\mathcal{N}_{\text{NN}}\{s\}}$, where $\mathcal{N}_{\text{NN}}\{s\}$ is the number of NN pairs of occupied sites in $\{s\}$.²¹

B. Eden rates: $k_j = \alpha k_0$, for $j \geq 1$

Here individual islands are Eden clusters.^{9,24} These have roughly circular large-size shape, with a weak (very) large-scale shape anisotropy reflecting lattice symmetry. Their radius R expands at a roughly constant rate determined by k_1 , and their active or growing zone width W scales like R^q with q between 0.32 and 0.5.⁹ Figure 3 shows occupied site distributions for various p values for a simulated lattice filling with $\alpha=499$. Clearly this α value is still too small for individual islands to have become nearly circular before coalescence.

Previous analyses have shown that the characteristic length satisfies $\xi_0 \sim c\alpha^\omega$ with $\omega = \frac{1}{3}$,^{8,22} as does the average radius for separated islands (at low p). There are fluctuations in island perimeters on a shorter length scale, $O(\xi_0)$. The large- α structure of this model, on a length scale $\xi_0 = O(\alpha^{1/3})$, is most conveniently characterized via continuum Johnson-Mehl type models:²⁵ grains nucleate at a constant rate at “unconverted” points in the plane; grains have an appropriate fixed nearly circular shape and expand at a constant rate; overlapping grains are re-

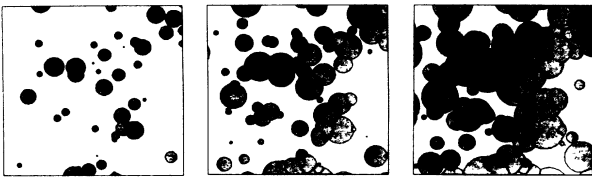


FIG. 4. Johnson-Mehl grain-growth patterns [provided by H. J. Frost, C. V. Thompson, and C. L. Howe (private communication)]. Circular grains nucleate at rate Γ , and expand radially at rate G . A fraction $p = 1 - \exp(-\pi\Gamma G^2 t^3/3)$ of the plane is converted at time t . Patterns shown for $p \approx 0.2, 0.53$, and 0.84 also indicate the curves along which grains first met.

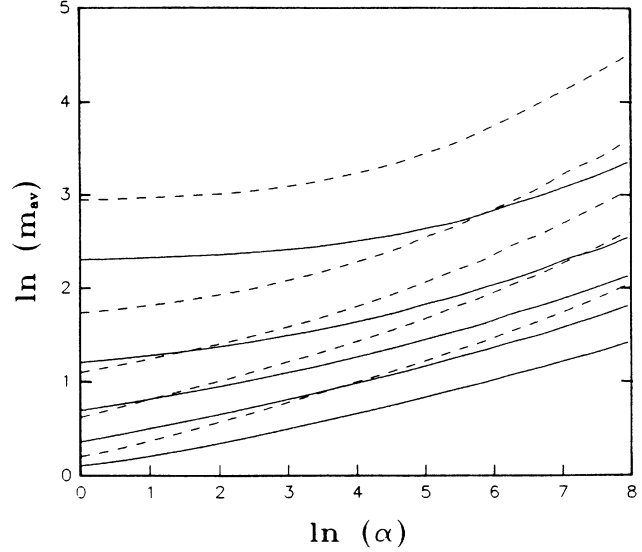


FIG. 5. Scaling of $m_{\text{av}}(i)$ with α for Eden rates. Solid (dashed) lines correspond to $i=1$ ($i=2$) for $p=0.1, 0.3, 0.5, 0.7$, and 0.9 (from bottom to top). The $\alpha = O(10^3)$ slopes, $(d/\ln\alpha)\ln m_{\text{av}}(i)$, range between 0.22 and 0.29 for $i=1$, and 0.31 and 0.40 for $i=2$.

garded as a single cluster (see Fig. 4). Such a continuum model, which ignores fluctuations in growth at the cluster perimeters, determines the large- α scaling functions shown in Eq. (2).

For Eden rates with $\alpha \lesssim O(10^3)$, $m_{\text{av}}(1)$ scales like $\alpha^{\bar{\omega}}$ with $\bar{\omega} \approx \frac{1}{5}$, rather than like ξ_0 or $\alpha^{1/3}$ (see Fig. 5). To understand this behavior, consider first the low- p regime of separated islands with $R = O(\xi_0) = O(\alpha^{1/3})$. Assume that the number of defects (holes, overhangs) encountered in a horizontal or vertical cross section of such an Eden cluster increases with R , such as, say, $O(R^q)$. These have the effect of reducing the $m_{\text{av}}(1)$ from $O(R)$ to $O(R^{1-q}) = O(\alpha^{(1-q)/3})$. The choice $\bar{q} = q$ seems consistent with the results of Fig. 5 and previous estimates of q . However, this agreement may be accidental since defects are associated more with the “intrinsic” active zone width, rather than with the long-wavelength fluctuations which generate the above-mentioned width scaling.²⁶ Thus \bar{q} may reflect an effective intrinsic width exponent for the “small” clusters associated with $\alpha \lesssim O(10^3)$. In contrast, $m_{\text{av}}(2)$ appears to scale more like ξ_0 or $\alpha^{1/3}$, for $\alpha \lesssim O(10^3)$ (see Fig. 5). This is expected since the contri-

TABLE III. The reciprocal effective dimension $\rho = 1/\bar{d}$ for occupied clusters generated by filling with Eden rates. Values for various α and $p/p_c(\alpha)$ are shown.

α	$\frac{1}{2}$	$\frac{p/p_c}{\frac{5}{6}}$	1
$\frac{1}{2}$	0.68	0.59	0.55
1	0.65	0.58	0.54
2	0.65	0.58	0.54
4	0.65	0.58	0.55
9	0.62	0.59	0.55
19	0.60	0.58	0.56

TABLE IV. $\lim_{s \rightarrow \infty} t/s$ for occupied clusters generated by filling with Eden rates. Values for various α and $p/p_c(\alpha)$ are shown.

α	$\frac{1}{2}$	$\frac{p/p_c}{\frac{5}{6}}$	1
$\frac{1}{2}$	1.30	0.91	0.67
1	1.23	0.89	0.69
2	1.19	0.86	0.69
4	1.10	0.85	0.69
9	0.97	0.78	0.66
19	0.88	0.72	0.61

bution from filled strings in the center of clusters should dominate here. [The average is now weighted by string length, unlike in $m_{av}(1)$.] Actually a more concise analysis of $\alpha \lesssim O(10^3)$ data reveals $m_{av}(2)$ scaling exponents slightly greater than $\frac{1}{3}$. However, it seems that this “finite-size” effect can also be explained (see Appendix A).

Results for the variation, with p and α , of $\rho = 1/\bar{d}$ and $\lim_{s \rightarrow \infty} t/s$ are shown in Tables III and IV, respectively. Data was obtained from 20 simulated fillings on a 200×200 site lattice with periodic-boundary conditions. The behavior observed parallels that described for the multiplicative rate choice, and the comments made there are again appropriate. For individual Eden clusters, t scales like R^δ when $\delta \downarrow 1$ slowly as $R \rightarrow \infty$, so $t/s \sim R^{\delta-2}$.²⁷ Correspondingly we expect $\lim_{s \rightarrow \infty} t/s$, for the filling process with Eden rates, to scale like $\alpha^{-(2-\delta)/3}$. The weights of the correlated animals associated with the $p \rightarrow 0$ behavior of these quantities are not as easily expressed as for multiplicative rates. For example, $s=4$ linear, T -shaped, and square animals have weights in proportion to $\frac{2}{3}\alpha^2 + \frac{1}{3}\alpha^3$, $\frac{1}{4}\alpha^2 + \frac{1}{2}\alpha^3$, and $\frac{1}{3}\alpha^2 + \frac{2}{3}\alpha^3$, respectively.

III. FINITE-SIZE-SCALING ANALYSIS OF PERCOLATION TRANSITIONS

Our analysis is based on the behavior of the second moment of the occupied cluster-size distribution, $M_L(p) = \sum_s s^2 n_s$ ($= p s_{av}$), for finite $L \times L$ lattices with periodic-boundary conditions (cf. Refs. 1 and 27). We assume that M_L has the finite-size-scaling form

$$M_L(p) \sim \xi_0^{2-\gamma/\nu} L^{2+\gamma/\nu} F((p-p_c)\xi_0^{-1/\nu} L^{1/\nu}), \quad (3)$$

where $F(z) \sim z^{-\gamma}$, as $z \rightarrow \infty$, recovering the correct $L = \infty$ scaling behavior. Here we have attempted to display the dominant dependence of F on the clustering parameter α explicitly through the ξ_0 dependence. Presumably there will be a weaker residual α dependence. From Eq. (3), the point of intersection of the ratio functions,

$$R_L(p) = M_{2L}(p)/M_L(p), \quad (4)$$

for different L , should approach p_c , as L increases. Their value at the point of intersection should approach $2^{2+\gamma/\nu}$ providing an estimate of γ/ν . An estimate of ν^{-1} is provided by $\log_2[(\partial/\partial p)R_{2L}/(\partial/\partial p)R_L]|_{p=p_c}$.

A parallel treatment is used to determine the critical occupancy p_c and critical exponents, associated with the percolation transition for unoccupied clusters. Analysis of either the occupied or unoccupied-site-percolation problems, could be based on the behavior of various non-local quantities other than that chosen above,²⁷ but resulting estimates of critical occupancies and exponents are typically no better.

Our determination of $M_L(p)$ corresponds to an unconventional ensemble average which is more suited to our computer simulation filling routine. The standard grand ensemble average of some quantity A for these filling processes is evaluated at fixed time t and has the form $\langle A \rangle_t = \sum_N \langle A \rangle_{N,t}$. Here $\langle A \rangle_{N,t} = \sum_{\{N\}} A_{\{N\}} F_{\{N\}}^{(N)}(t)$, where $F_{\{N\}}^{(N)}(t)$ denotes the probability of finding exactly N sites $\{N\}$ occupied at time t , and $A_{\{N\}}$ is the corresponding value of A . After determining the time dependence of the occupancy $p = \langle p \rangle_t$, one can eliminate t to obtain $\langle A \rangle_t$ as a function of p . The random percolation analysis of Saleur and Derrida²⁷ corresponds to this procedure. However, instead we sample at fixed N , i.e., we use

$$\langle A \rangle_N = \lim_{T \rightarrow \infty} \int_0^T dt \langle A \rangle_{N,t} / \int_0^T dt \langle 1 \rangle_{N,t}.$$

This automatically gives the $p = N/L^2$ dependence of this average of A for discrete p values. We then interpolate between these discrete values to obtain a function of a continuous variable p . The two procedures only agree in the $L \rightarrow \infty$ limit, which is sufficient for our purposes.

Figure 6 displays ratio function plots (R_L versus p) for occupied clusters, obtained from our procedure, for $\alpha = 1$

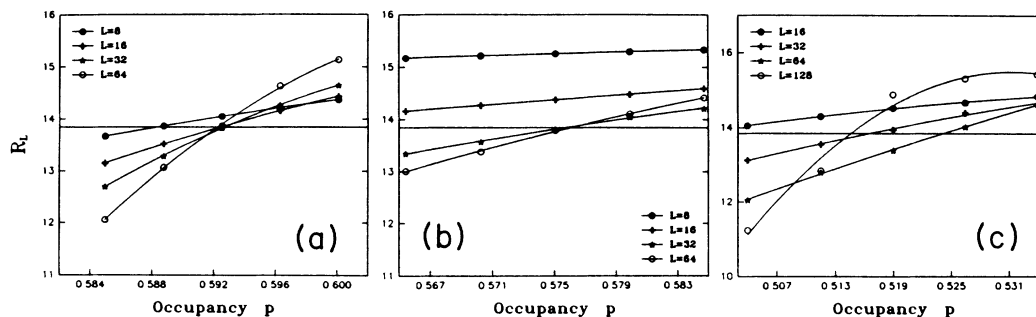


FIG. 6. Ratio functions $R_L(p) = M_{2L}(p)/M_L(p)$ for (a) $\alpha=1$ random filling, (b) $\alpha=9$ multiplicative rates, and (c) $\alpha=49$ Eden rates. A horizontal line at $2^{2+\gamma/\nu} \approx 13.85$, for random percolation critical exponents, is also shown.

TABLE V. Estimates of p_c (and γ/ν) for percolation of occupied clusters obtained from the crossing point of ratio functions R_L and R_{2L} . Values for various L and α are shown for both multiplicative and Eden rates (γ/ν values are in parentheses).

α	Multiplicative			Eden		
	8	16	32	8	16	32
$\frac{1}{100}$		0.615 (1.79)		0.643 (1.78)	0.645 (1.81)	0.645 (1.80)
$\frac{1}{5}$	0.658 (1.79)	0.660 (1.81)	0.656 (1.71)	0.628 (1.83)	0.622 (1.76)	0.621 (1.74)
$\frac{1}{2}$	0.645 (1.78)	0.646 (1.80)	0.644 (1.70)	0.611 (1.83)		0.605 (1.74)
1	0.598 (1.84)	0.593 (1.80)	0.592 (1.78)	0.598 (1.84)	0.593 (1.80)	0.592 (1.78)
2			0.553 (1.80)		0.576 (1.78)	0.575 (1.76)
4						0.556 (1.69)
9			0.577 (1.80)		0.549 (1.83)	0.542 (1.76)
19		0.633 (1.88)				
49						0.509 (1.65)

random filling, $\alpha=9$ multiplicative rates, and $\alpha=49$ Eden rates. The $\alpha=1$ behavior deviates slightly from that of Ref. 27, for reasons described above. Behavior of the unoccupied cluster ratio functions is similar, except that they have negative slopes. In Table V we have given p_c (p'_c) values, and corresponding estimates of γ/ν , for occupied clusters, obtained from the crossing of various ratio functions. Table VI shows corresponding results for unoccupied clusters. These estimates for γ/ν strongly

suggest that these cooperative filling models are always in the random percolation universality class (where $\nu=\frac{4}{3}$, $\gamma=\frac{43}{18}$).¹ Consequently we obtain alternative estimates of critical occupancies by determining where the appropriate ratio functions equal the random percolation value for $2^{2+\gamma/\nu}\approx 13.85$. See Table VII for corresponding p_c and p'_c values. Direct estimates of ν from R_L slope behavior are quite sensitive to statistical fluctuations, and are not given here.

TABLE VI. Estimates of p'_c (and the corresponding γ/ν) for percolation of unoccupied clusters obtained from the crossing point of appropriate ratio functions R_L and R_{2L} . Values for various L and α are shown for both multiplicative and Eden rates (γ/ν values are in parentheses).

α	Multiplicative			Eden		
	8	16	32	8	16	32
$\frac{1}{100}$	0.369 (1.86)	0.373 (1.79)		0.372 (1.85)	0.374 (1.81)	0.374 (1.82)
$\frac{1}{5}$	0.353 (1.80)	0.355 (1.78)	0.352 (1.83)	0.379 (1.80)	0.380 (1.79)	0.382 (1.75)
$\frac{1}{2}$	0.371 (1.81)	0.371 (1.82)	0.373 (1.70)	0.392 (1.82)	0.394 (1.81)	0.399 (1.72)
1	0.402 (1.83)	0.405 (1.81)	0.409 (1.72)	0.402 (1.83)	0.405 (1.81)	0.409 (1.72)
2			0.463 (1.78)			
4						0.427 (1.71)
9			0.564 (1.86)		0.420 (1.84)	0.429 (1.76)
19		0.592 (1.91)				0.437 (1.78)
49						0.444 (1.75)

TABLE VII. Estimates of p_c obtained from the solution of $R_L(p) = 2^{2+\gamma/\nu} \approx 13.85$, using random percolation critical exponents, and from $L \rightarrow \infty$ extrapolation (assuming linearity in L^{-2}). Corresponding estimates of p'_c are given in parentheses. Results for both multiplicative and Eden rates are shown for various values of α . We estimate the uncertainty of the finite L results at ± 0.002 , except for a few large L and α cases where it is roughly four times larger.

α	Multiplicative L						Eden L					
	8	16	32	64	129	EXT	8	16	32	64	128	EXT
$\frac{1}{100}$	(0.375)	(0.372)	(0.373)			(0.372)	(0.379)	(0.376)	(0.375)	(0.375)		(0.375)
	0.621	0.615	0.615			0.614	0.644	0.644	0.644	0.644		0.644
$\frac{1}{5}$	(0.354)	(0.354)	(0.354)	(0.353)		(0.354)	(0.380)	(0.380)	(0.380)	(0.380)		(0.380)
	0.659	0.658	0.659	0.658		0.659	0.623	0.625	0.624	0.622		0.624
$\frac{1}{2}$	(0.374)	(0.373)	(0.372)	(0.373)		(0.373)	(0.395)	(0.396)	(0.395)	(0.397)		(0.396)
	0.646	0.645	0.646	0.644		0.645	0.604	0.606	0.608	0.607		0.608
1	(0.411)	(0.407)	(0.406)	(0.409)		(0.408)	(0.411)	(0.407)	(0.406)	(0.409)		(0.408)
	0.588	0.592	0.593	0.592		0.593	0.588	0.592	0.593	0.592		0.593
2		(0.465)	(0.462)	(0.463)		(0.462)	(0.421)	(0.414)	(0.422)	(0.413)		(0.416)
		0.548	0.552	0.553		0.553	0.571	0.578	0.577	0.576		0.578
4		(0.533)	(0.524)	(0.521)		(0.520)		(0.424)	(0.421)	(0.424)		(0.422)
		0.542	0.551	0.554		0.554	0.552	0.558	0.565	0.561		0.563
9			(0.580)	(0.574)		(0.572)		(0.431)	(0.426)	(0.428)		(0.427)
			0.576	0.576		0.576		0.541	0.545	0.543		0.545
19				(0.618)	(0.613)	(0.611)		(0.441)	(0.434)	(0.435)		(0.434)
				0.612	0.613	0.613		0.522	0.531	0.528		0.531
49									(0.448)	(0.438)	(0.441)	(0.438)
									0.517	0.524	0.515	0.519

Figure 7 (Fig. 8) shows diagrammatically the α dependence of p_c and p'_c for multiplicative (Eden) rates. Increased propensity for clustering initially causes p_c to drop (i.e., as α increases above unity), as might be expected from corresponding Ising-model analyses. However, for multiplicative rates, one clearly sees an increase in p_c , for larger α . Our results suggest that an analogous turn around also occurs for Eden rates, but at much larger α ($p_c = 0.52$, for $\alpha = 499$). We explain this behavior as follows. The $\alpha = \infty$ "continuum" processes generate occu-

ried areas with smooth perimeters. Reducing α from infinity *roughens* the edges of occupied regions (relative to the length scale, ξ_0). We argue (see Sec. IV) that this has the effect of enhancing percolation, i.e., lowering p_c . The $\alpha \rightarrow \infty$ limiting behavior is achieved more slowly for Eden rates, since the corresponding cluster perimeters are much rougher. We expect that the $\alpha \rightarrow \infty$ value of p_c for Eden rates is comparable to the $\alpha \rightarrow \infty$ value of ~ 0.69 for multiplicative rates (see Sec. VI).

Another clear trend in the results for multiplicative

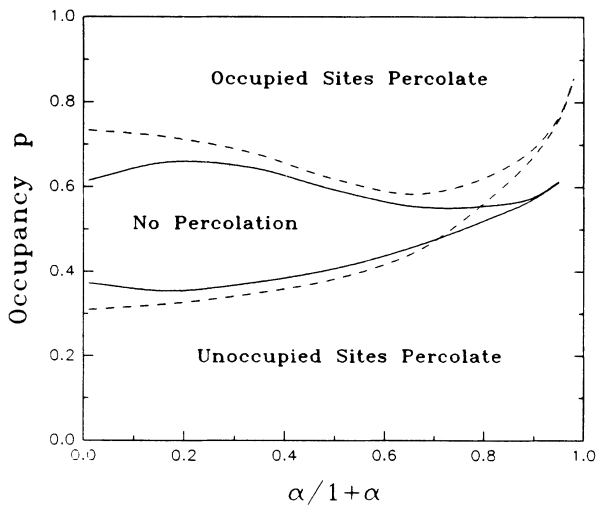


FIG. 7. α dependence of percolation thresholds for occupied (p_c) and unoccupied (p'_c) clusters for multiplicative rates. Accurate finite-size-scaling results (solid lines), and 2×2 cell renormalization-group results (dashed lines) are shown.

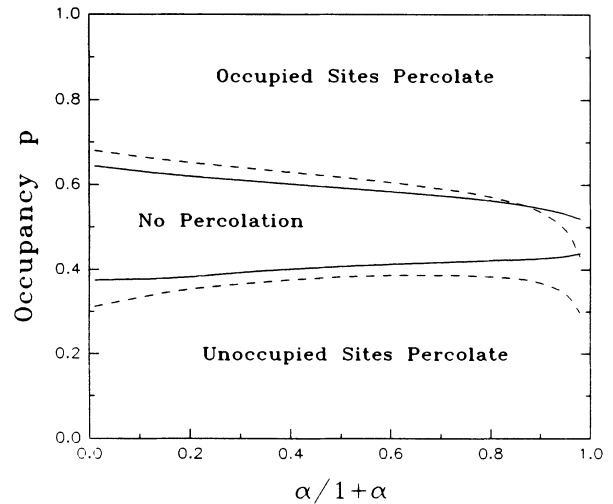


FIG. 8. α dependence of percolation thresholds for occupied (p_c) and unoccupied (p'_c) clusters for Eden rates. Accurate finite-size-scaling results (solid lines), and 2×2 cell renormalization-group results (dashed lines) are shown.

rates is that $p'_c \sim p_c$, as $\alpha \rightarrow \infty$. Our results for Eden rates also reflect this trend (for $\alpha=499$, $p_c=0.52$, and $p'_c=0.49$, so $p_c - p'_c$ has dropped significantly from its value for $\alpha=49$). This is a consequence of the property that for any ($\alpha = \infty$) continuum percolation problem, the disappearance of “unoccupied” percolating regions and appearance of “occupied” regions occur simultaneously, i.e., $p'_c = p_c$.²⁸ It is interesting to compare behavior observed here to that of the two-dimensional Ising model where $p'_c = 1 - p_c$. There $p'_c \sim p_c \sim \frac{1}{2}$ only at the critical point (where the characteristic or correlation length diverges).³ See Ref. 12 for a more detailed comparison.

It is appropriate here to comment briefly on the significance of the $\alpha \rightarrow 0$ strongly anticlustering behavior also shown in Figs. 7 and 8. For multiplicative rates, $\alpha \rightarrow 0$ corresponds to “random” filling in stages of sites with zero, one, two, three, then four occupied NN sites. These stages end at occupancies $p = 0.364$, 0.476 , ~ 0.52 , ~ 0.64 , and 1 , respectively.⁸ For Eden rates, $\alpha \rightarrow 0$ corresponds to random filling of sites with no occupied NN up to $p = 0.364$ (as for multiplicative rates), followed by random filling of the remaining sites. Our results show that (i) unoccupied clusters cease to percolate shortly after the first stage (in both cases) and (ii) occupied clusters percolate in the fourth stage for multiplicative rates (filling of sites with three occupied NN).

Also shown in Figs. 7 and 8 are the results of real-space renormalization-group calculations for a 2×2 cell using a horizontal spanning rule.²⁹ Behavior is qualitatively similar to the finite-size-scaling results, except for high α . This renormalization-group theory preserves the inequality $p'_c \leq p_c$, and also illustrates quite clearly why the asymptotic behavior $p'_c \sim p_c$ is seen so quickly for multiplicative rates as α increases (see Appendix B).

IV. EFFECT OF ISLAND PERIMETER ROUGHNESS ON PERCOLATION THRESHOLDS

It was suggested above that increased island perimeter roughness (i.e., increased island “fuzziness”) enhances percolation, i.e., lowers p_c . A crude assessment of this affect goes as follows. Consider the variation of the percolation threshold $p_c(W)$ for a family of filling processes where individual islands have the same shape and average radial dimension R , but differing active zone widths W . (R and W should be interpreted here as near- p_c values.) This shape is associated with the convex envelope of individual islands. Our key assumption is that percolation is essentially determined by the corresponding envelope encompassing clusters of coalesced islands. One then expects that $p_c(0) - p_c(W) = O(W/R) > 0$ since increasing W from 0 (without changing this envelope) reduces p by $O(W/R)$. This result suggests that p_c should approach its $\alpha \rightarrow \infty$ limit such as $\alpha^{-1/2}$ for multiplicative rates, and $\alpha^{-(1-q)/3} \sim \alpha^{-1/5}$ for Eden rates [for $\alpha \lesssim O(10^3)$]. This behavior is compatible with (but not confirmed by) the limited results of Sec. III.

Here we present a systematic analysis of the effect on p_c of smoothing the perimeters of islands generated by an Eden rate choice. Smoothing is achieved by a multiple-hit noise reduction method developed recently to assist

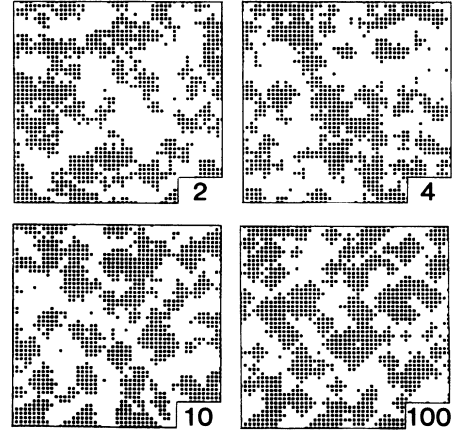


FIG. 9. Typical occupied site distributions, at $p = \frac{1}{2}$, for filling with $\alpha=49$ Eden rates, and multiple-hit (M) noise reduction. Various M values are shown.

analysis of growing zone width scaling and lattice anisotropy effects.²⁶ Specifically we analyze the following model: island nucleation occurs at sites with no occupied NN at rate k_0 as previously; sites with $j \geq 1$ occupied NN are “hit” at rate $k_j = M \alpha k_0$, and fill after the M th hit. Thus $M = 1$ recovers the original Eden rate choice, and $M > 1$ has the effect of smoothing island perimeters while preserving average island size. It is easy to see that as $M \rightarrow \infty$, individual island growth occurs layerwise (cf. Ref. 26) producing diamond-shaped islands. Thus increasing M does change island shape. Figure 9 shows typical $p = \frac{1}{2}$ occupied site distributions for $\alpha=49$ and various M values.

Figure 10 displays results from finite-size-scaling calculations indicating the dramatic increase of p_c with M , for fixed $\alpha=49$. Note that p_c versus $1/M$ is roughly linear for large M (the intrinsic width W scales as $1/M$).²⁶

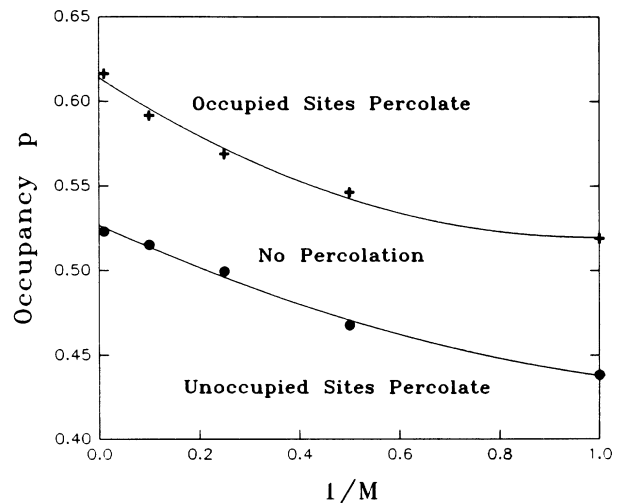


FIG. 10. M dependence of the percolation thresholds for occupied (+) and unoccupied (●) clusters for filling with $\alpha=49$ Eden rates and multiple-hit (M) noise reduction.

These results also show that $p_c - p'_c$ changes little as M increases. This is not too surprising since increasing M does not increase the average linear island size, and thus does not achieve a continuum limit. Finally we mention that our calculations suggest that all these $M \geq 1$ models have random percolation critical exponents.

V. SPREADING AND WALKING REPRESENTATIONS FOR CLUSTERS AND THEIR PERIMETERS

It is well known that one can “grow” an individual random percolation cluster, for occupancy p , via a variety of “spreading algorithms”:³⁰ start with a single occupied site surrounded by adjacent “growth” sites; choose a growth site (in one of various ways); either occupy it with probability p and convert any unspecified adjacent sites to growth sites, or make it permanently unoccupied with probability $1-p$; continue choosing another growth site, etc. If correlations are present, the probability of occupying (making permanently unoccupied) the chosen growth site does not equal $p(1-p)$, but rather the *conditional* probability that this site be occupied (unoccupied) *given* the state of all previously occupied cluster sites and those growth sites assigned permanently unoccupied. (These conditional probabilities must be determined from appropriate distributions with occupancy p .)

For irreversible cooperative filling models, these conditional probabilities depend *nontrivially* on all specified occupied cluster and unoccupied perimeter sites. Since there are infinitely many such quantities (and they cannot be determined exactly), exact implementation of these spreading algorithms is impossible. However one expects that the dependence of these conditional probabilities on distant specified sites is weak. Thus approximate spreading algorithms might be developed incorporating a corresponding finite subset of conditional probabilities.

Analogous spreading algorithms can be used to generate clusters of unoccupied sites. In fact the situation is slightly better here since walls of empty sites (of thickness two) shield sites on one side from the influence of those on the other.⁸ This reduces or removes the influence of certain distant specified sites on the conditional probabilities determined spreading. However, infinitely many such quantities are still required.

Next we consider algorithms for directly generating connected cluster perimeters. Note that external (internal) perimeters of occupied clusters correspond to internal (external) perimeters of unoccupied clusters. We first recall the procedure of Ziff, Cummings, and Stell³¹ for systematically walking around such perimeters: start with an adjacent unoccupied/occupied pair of sites; move to the occupied site and look in the left, forward, right and then reverse directions until another occupied site is found; move to this site and search for an adjacent occupied site as above; continue until the starting point is passed in the same direction as originally. The key realization of Ziff, Cummings, and Stell³¹ was that, for random percolation, the cluster whose perimeter is being considered could be generated during (rather than prior to) this walk: each time the state of an unspecified site is required, it is chosen occupied (unoccupied) with proba-

bility $p(1-p)$. Thus the perimeter is generated directly as a type of self-avoiding walk.

Again the presence of correlations complicates the perimeter generating algorithm. Now the state of an unspecified site must be chosen according to the *conditional probability* that the site is occupied or unoccupied *given* the state of all previously specified adjacent occupied and/or unoccupied perimeter sites. (These conditional probabilities must be determined from appropriate distributions with occupancy p .) Thus the perimeter is generated as a type of *correlated self-avoiding walk*. Consider this procedure for island-forming or clustering systems with correlation lengths ξ_0 of many lattice vectors. Clearly the correlations present will tend to “straighten out” the cluster perimeters relative to the random percolation case. Also for low occupancies, one expects the walks to typically map out the perimeters of individual growing islands.

Exact implementation of this algorithm is generally impossible for irreversible cooperative filling (or other two-dimensional models) because of the infinite number of conditional probabilities required. However, approximate implementation, neglecting the effect of “distant” sites, should be instructive. The limitations of such approximations should be evident in “how well” the perimeter closes on itself. These investigations are left for later work.

VI. CONCLUSIONS AND EXTENSIONS

Finite-size-scaling techniques and direct cluster structure analysis have been successfully applied to provide detailed information on the percolative properties of models involving irreversible cooperative lattice filling on a square lattice. These techniques, and several observations made here, should have broader applicability. For example, various models describing nucleation, growth and coalescence of islands should display the following features: percolation problems for occupied and unoccupied clusters will be distinct; as the island-forming propensity is “switched on” and then increased, p_c may first drop but later increase as island perimeter roughness decreases (relative to the characteristic length) and the large island size continuum limit is approached. One also expects $p_c - p'_c$ to vanish in this limit. The spreading and walking algorithms described in Sec. V for direct generation of clusters and perimeters also have general applicability. Below are comments on various modifications and extensions to the models and analyses presented here.

(i) *Analysis of pair connectivities* p_{ij} (probabilities that various pairs $\{ij\}$ of sites are in the same cluster) provides another approach to the investigation of percolative properties.¹ For an equilibrated lattice gas with pairwise additive interactions u_{ij} , density (i.e., occupancy) expansions for the p_{ij} can be readily obtained, based on a straightforward decomposition of the graphical expansion for the corresponding pair probabilities.³² Analogous graphical expansions are available for pair probabilities in irreversible cooperative filling models where the rate for filling site i has the form $\prod_j (1 + \tilde{f}_{ij})$, j ranging over occupied sites.²¹ Now the bonds in graphs represent

\tilde{f}_{ij} , rather than $f_{ij}=1-e^{-\beta u_{ij}}$ as in the equilibrium theory. However, the \tilde{f} graphs have different weights than the f graphs, and decomposition parallel to the above equilibrium procedure fails to produce correct expressions for pair connectivities.

(ii) *Heterogeneous nucleation of islands* (about seeds) provides a natural modification to the above homogeneous or continuous nucleation models. As the seed density ϵ is lowered, the average size of islands (for any p) increases, so $\epsilon \rightarrow 0$ produces a continuum limit (analogous to $\alpha \rightarrow \infty$ in the homogeneous nucleation models). Consider the Eden rate choice ($k_0=0$, k_i equal for $i \geq 1$) where roughly circular Eden clusters grow about randomly distributed seeds. Figure 11 shows corresponding occupied site distributions for $\epsilon=0.0026$. As ϵ is lowered below the random percolation critical occupancy of 0.593, we expect that p_c will first drop below 0.593, and then increase dramatically to its $\epsilon \rightarrow 0$ continuum limit. In this limit, $p_c = p'_c$ should be close to 0.68, the value of the critical area fraction for the continuum percolation problem where perfect circles expand, at constant rate, about randomly distributed seeds³³ (see Fig. 12). If circles are replaced by squares, a similar estimate for p_c is obtained.³³ Note that this p_c value is also similar to that obtained for homogeneous nucleation with rates $k_i \propto \alpha^i$, as $\alpha \rightarrow \infty$.

(iii) *Polychromatic irreversible cooperative filling*. Suppose that the sites of a square lattice are filled irreversibly to attain one of two states or "colors," x or y .³⁴ The corresponding filling rates k^x and k^y in general differ, and might depend, e.g., on the state of NN sites. Clusters are defined by NN connectivity, as previously. One could look for possible percolation transitions of either x or y clusters (but not both) during filling, or percolation transitions in a family of *saturation states* generated by varying a bias in the filling rates for one species relative to the other.

Consider now the class of processes with "symmetric" filling rate choices, so that the statistics of x and y sites are identical. Clearly neither x or y clusters percolate in the saturation states. Here we ask whether increasing the propensity for x - x and y - y (but not x - y) clustering, shifts the saturation state "closer" to percolating? We consider only an Eden rate choice: $k^x(k^y)=k_0$ if no NN x (y) sites, $k^x(k^y)=\alpha k_0$ if one or more NN x (y) sites. The $\alpha \rightarrow \infty$ continuum limit corresponds to a two-state Johnson-Mehl type model.^{12,22,35} grains nucleate at constant rate at unconverted points in the plane; each is ran-

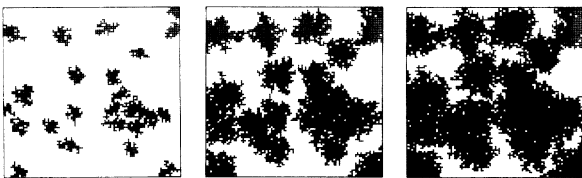


FIG. 11. Growth of Eden clusters about randomly distributed seeds of density $\epsilon=0.0026$: typical occupied site distributions for $p=0.15, 0.5$, and 0.7 .

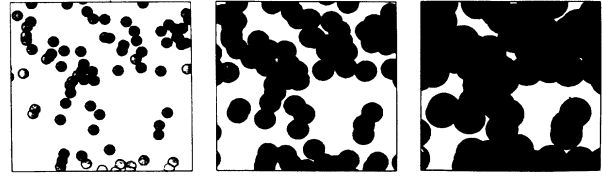


FIG. 12. Patterns for expansion of circular grains about randomly distributed seeds [provided by H. J. Frost, C. V. Thompson, and C. L. Howe (private communication)]. For seed density E and radial expansion rate G , a fraction $p=1-\exp(-\pi EG^2 t^2)$ of the plane is converted at time t . Patterns shown for $p \approx 0.18, 0.54$, and 0.83 also indicate the straight line segments along which grains first met.

domly assigned an x or y color; they have the appropriate nearly circular shape, and expand at constant rate; upon meeting grains merge if of like color, and form a permanent x - y boundary otherwise. This model also describes the continuum limit of a model for formation of two-phase $c(2 \times 2)$ clusters via irreversible filling with Eden rates.^{12,22} We have noted previously the equivalence of this model to a site percolation problem on a random "Johnson-Mehl"-type lattice with effective coordination number equal to six. This observation, together with more general arguments, imply that the $\alpha \rightarrow \infty$ model is at the percolation threshold for both x and y clusters.^{22,36}

(iv) *Irreversible reaction models*, where two species first adsorb and then immediately react irreversibly, exhibit interesting kinetic transitions.^{19,37} They provide a natural extension of the models described in (iii). For the latter, in general, the saturation state is *not* at the percolation threshold, and the corresponding effective cluster dimension is typically below the universal random percolation threshold value. However, modification (and complication) of the model by inclusion of a reaction may result in quasi-steady-state clusters with this universal dimension.¹⁹

(v) *A continuous Johnson-Mehl-type percolation problem* has been associated with the $\alpha \rightarrow \infty$ continuum limit of lattice filling with Eden rates (Sec. II B). A similar connection was made for polychromatic filling with Eden rates. Various modifications of Johnson-Mehl grain growth problems are possible, e.g., to include a declining nucleation rate, or nucleation exclusion zones about growing grains.³⁸ The associated continuum percolation problems are expected to be in the random percolation universality class. We have begun a direct analysis of these.³⁹

ACKNOWLEDGMENTS

One of us (J.W.E.) was supported for this work by the Ames Laboratory Applied Mathematical Sciences Program. Ames Laboratory is operated for the U.S. Department of Energy by Iowa State University under Contract No. W-7405-ENG-82. This work was supported by the Office of Basic Energy Sciences.

APPENDIX A: CHARACTERISTIC LENGTH SCALING

Consider processes involving nucleation, growth, and coalescence of islands where the rate of growth \dot{R} of the "radial dimension" R of an individual island scales like $R^\Delta \alpha$. Next determine the island nucleation rate (Γ), and "radial" growth rate (G) measured in units of the characteristic size ξ_0 . Clearly one has $\Gamma \sim \xi_0^{-2}$ and $G \sim \xi_0^{-1} \xi_0^\Delta \alpha$, so $G/\Gamma \sim \xi_0^{\Delta-3} \alpha$. In the large- α scaling regime, we assume that distributions with different α are self-similar. Then the ratio G/Γ should be invariant, which implies that $\xi_0 \sim \alpha^{-\omega}$, with $\omega = 1/(3-\Delta)$. This recovers stated results for multiplicative ($\Delta=1$) and Eden ($\Delta=0$) rate choices.

We now suggest why "effective" ω slightly greater than $\frac{1}{3}$ was observed in the $\alpha \lesssim O(10^3)$ $m_{av}(2)$ results, for the Eden rate choice. For an individual Eden cluster, the total number of sites s_E and perimeter sites t_E satisfy $s_E \sim R^2$ and $t_E \sim R^\delta$, where $\delta \downarrow 1$ slowly, as $R \rightarrow \infty$.⁴⁰ Since $\dot{s}_E = k_1 t_E$, it follows that \dot{R} scales like $k_1 R^{\delta-1}$, so $\Delta = \delta - 1 \downarrow 0$, slowly (as $\alpha \rightarrow \infty$).

APPENDIX B: SMALL-CELL REAL-SPACE RENORMALIZATION-GROUP CALCULATIONS

Let $R_1^x(p)$ [$R_1^0(p)$] denote the probability that the occupied [unoccupied] sites span a $b \times b$ cell in a fixed (say, horizontal) direction, for a lattice with a fraction p of sites occupied (cf. Ref. 30). For our irreversible cooperative filling models, formal expansion demonstrates that²¹

$R_1^x = O(p^b)$ and $R_1^0 = 1 - O(p^b)$, as $p \rightarrow 0$. We assume that $R_1^x(p)$ crosses p once (from below, for increasing p) for $0 < p < 1$. This value of p on crossing provides an estimate of p_c . Similarly, we assume that $R_1^0(p)$ crosses $1-p$ once (from above, for increasing p) for $0 < p < 1$, providing an estimate of p'_c .

Clearly one has $R_1^x + R_1^0 = 1 + P_{2h} - P_{0h}$, where P_{2h} (P_{0h}) denotes the probability that both (neither) occupied and unoccupied sites span horizontally. Next note that $P_{0h} = P_{2v} + P_{0hv}$, where P_{2v} is the probability that both occupied and unoccupied sites span vertically, and P_{0hv} is the probability that neither span horizontally or vertically. Then since $P_{2v} = P_{2h}$ by rotational symmetry, one finds that $R_1^x + R_1^0 = 1 - P_{0hv}$. Since this sum is less than unity, it follows that $p'_c < p_c$, when estimated as described above. It is also clear that the smaller P_{0hv} (relative to $|R_1^x - p|$ or $|R_1^0 - (1-p)|$), the closer p'_c to p_c . Note that $b \times b$ cell configurations contributing to P_{0hv} must include at least one subconfiguration ${}_{x0}^{0x}$ or ${}_{0x}^{x0}$. For cooperative filling with multiplicative rates, such subconfigurations are relatively rare (the empty sites fill "quickly" with rate k_2 or faster), and so $p_c \sim p'_c$, even for "moderate" α .

Results are presented in Figs. 7 and 8 only for 2×2 cells ($b=2$). Even here many equivalent forms are available for R_1^x and R_1^0 . One useful form is $R_1^x = p + P[{}_{xx}^{x0}] - P[{}_{00}^{0x}] - P[{}_{x0}^{0x}]$ and $R_1^0 = 1 - p - P[{}_{xx}^{x0}] + P[{}_{00}^{0x}] - P[{}_{x0}^{0x}]$, so $R_1^x + R_1^0 = 1 - 2P[{}_{x0}^{0x}]$. Here, the P 's indicate probabilities of the configurations shown.

¹D. Stauffer, Phys. Rep. **54**, 1 (1979); *Introduction to Percolation Theory* (Taylor and Francis, London, 1985).
²S. Kirkpatrick, in *Ill-Condensed Matter*, edited by R. Balian, R. Maynard, and G. Toulouse (North-Holland, Amsterdam, 1979).
³For a review, see D. Stauffer, A. Coniglio, and M. Adam, in *Advances in Polymer Science* (Springer-Verlag, Berlin, 1982), Vol. 44.
⁴F. Peruggi, Physica **141A**, 140 (1987); F. Peruggi, F. di Liberto, and G. Monroy, *ibid.* **123A**, 175 (1984).
⁵J. Kertesz, B. K. Chakrabarti, and J. A. M. S. Duarte, J. Phys. A **15**, L13 (1982).
⁶J. L. Lebowitz and H. Saleur, Physica **138A**, 194 (1986).
⁷J. W. Evans, J. Phys. A **20**, 6487 (1987).
⁸J. W. Evans, J. A. Bartz, and D. E. Sanders, Phys. Rev. A **34**, 1434 (1986); J. W. Evans, D. R. Burgess, and D. K. Hoffman, J. Chem. Phys. **79**, 5011 (1983); P. Meakin, J. L. Cardy, E. Loh, and D. J. Scalapino, *ibid.* **86**, 2380 (1987).
⁹Z. Racz and M. Plischke, Phys. Rev. A **31**, 985 (1985); P. Freche, D. Stauffer and H. E. Stanley, J. Phys. A **18**, L1163 (1985); D. E. Wolf, *ibid.* **20**, 1251 (1987).
¹⁰M. E. Fisher, J. Math. Phys. **2**, 620 (1961).
¹¹R. M. Ziff, Phys. Rev. Lett. **56**, 545 (1986).
¹²J. W. Evans and D. E. Sanders, J. Vac. Sci. Technol. A **6**, 726 (1988); J. W. Evans, J. Chem. Phys. **87**, 3038 (1987).
¹³M. G. Lagally, G.-C. Wang, and T.-M. Lu, CRC Crit. Rev. Solid State Mater. Sci. **7**, 233 (1978).
¹⁴J. W. Evans, R. S. Nord, and J. A. Rabaey, Phys. Rev. B **37**,

8598 (1988).
¹⁵K. Binder, Solid State Commun. **34**, 191 (1980); E. D. Williams, W. H. Weinberg, and A. C. Sobrero, J. Chem. Phys. **76**, 1150 (1982).
¹⁶P. J. Estrup, in *Chemistry and Physics of Solid Surfaces*, Vol. 35 of *Springer Series in Chemical Physics*, edited by R. Vanselow and R. Howe (Springer, Berlin, 1984).
¹⁷R. Opila and R. Gomer, Surf. Sci. **112**, 1 (1981); J. W. Evans and H. Pak, *ibid.* **199**, 28 (1988).
¹⁸M. Rocca, H. Ibach, S. Lehwald, and T. S. Rahman, in *Structure and Dynamics of Surfaces I*, edited by W. Schommers and P. von Blanckenhagen (Springer, Berlin, 1986).
¹⁹R. M. Ziff and K. Fichtorn, Phys. Rev. B **34**, 2038 (1986).
²⁰*Epitaxial Growth*, edited by J. W. Mathews (Academic, New York, 1975).
²¹D. K. Hoffman, J. Chem. Phys. **65**, 95 (1976); J. W. Evans, Physica **123A**, 297 (1984).
²²J. W. Evans and R. S. Nord, J. Vac. Sci. Technol. **A5**, 1040 (1987).
²³E. Stoll and C. Domb, J. Phys. A **12**, 1843 (1979); A. Coniglio and L. Russo, *ibid.* **12**, 545 (1979).
²⁴M. Eden, in *Proceedings of the Fourth Berkeley Symposium on Mathematical Statistics and Problems*, edited by F. Neyman (University of California Press, Berkeley, 1961), Vol. IV.
²⁵W. A. Johnson and R. F. Mehl, Trans AIME **135**, 416 (1939); J. L. Meijering, Phillips Res. Rep. **8**, 270 (1953).
²⁶D. E. Wolf and J. Kertesz, J. Phys. A **20**, L257 (1987); J. Kertesz and D. E. Wolf, J. Phys. A **21**, 747 (1988).

- ²⁷H. Saleur and B. Derrida, *J. Phys. (Paris)* **46**, 1043 (1985).
- ²⁸R. Zallen and H. Scher, *Phys. Rev. B* **4**, 4471 (1971); J. Kertesz, *J. Phys. Lett.* **42**, L393 (1981).
- ²⁹P. J. Reynolds, H. E. Stanley, and W. Klein, *Phys. Rev. B* **21**, 1223 (1980).
- ³⁰A. Bunde, H. J. Hermann, A. Margolina, and H. E. Stanley, *Phys. Rev. Lett.* **55**, 653 (1985); P. Grassberger, *J. Phys. A* **18**, L215 (1983).
- ³¹R. M. Ziff, P. T. Cummings, and G. Stell, *J. Phys. A* **17**, 3009 (1984).
- ³²A. Coniglio, U. De Angelis, and A. Forlani, *J. Phys. A* **10**, 1123 (1977).
- ³³G. E. Pike and C. H. Seager, *Phys. Rev. B* **10**, 1421 (1974); S. W. Haan and R. Zwanzig, *J. Phys. A* **10**, 1547 (1977); E. T. Gawlinski and H. E. Stanley, *ibid.* **14**, L291 (1981).
- ³⁴J. W. Evans, D. K. Hoffman, and D. R. Burgess, *J. Chem. Phys.* **80**, 936 (1984); J. W. Evans and R. S. Nord, *Phys. Rev. B* **31**, 1759 (1985).
- ³⁵S. Ohta, K. Ohta, and K. Kawasaki, *Physica* **140A**, 478 (1987).
- ³⁶J. W. Evans and D. E. Sanders, *Phys. Rev. B* (to be published).
- ³⁷R. M. Ziff, E. Gulari, and Y. Barshad, *Phys. Rev. Lett.* **56**, 2553 (1986); P. Meakin and D. J. Scalapino, *J. Chem. Phys.* **87**, 731 (1987).
- ³⁸H. J. Frost and C. V. Thompson, *Acta Metall.* **35**, 529 (1987).
- ³⁹H. J. Frost and J. W. Evans (unpublished).
- ⁴⁰P. Meakin and T. A. Witten, *Phys. Rev. A* **28**, 2985 (1983).



FIG. 1. Filling with multiplicative rates for $\alpha=19$: typical occupied site distributions for $p=0.2$, 0.6 (near p_c), and 0.8 .

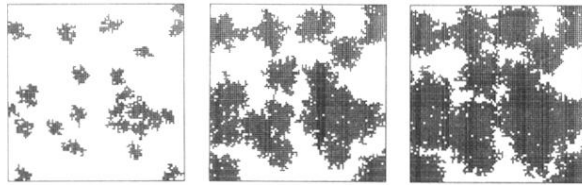


FIG. 11. Growth of Eden clusters about randomly distributed seeds of density $\varepsilon=0.0026$: typical occupied site distributions for $p=0.15, 0.5$, and 0.7 .

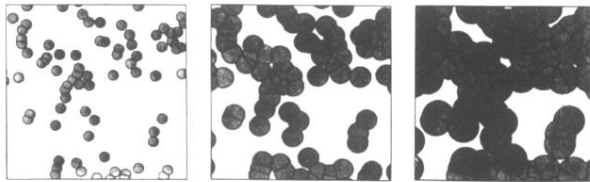


FIG. 12. Patterns for expansion of circular grains about randomly distributed seeds [provided by H. J. Frost, C. V. Thompson, and C. L. Howe (private communication)]. For seed density E and radial expansion rate G , a fraction $p = 1 - \exp(-\pi EG^2 t^2)$ of the plane is converted at time t . Patterns shown for $p \approx 0.18, 0.54,$ and 0.83 also indicate the straight line segments along which grains first met.

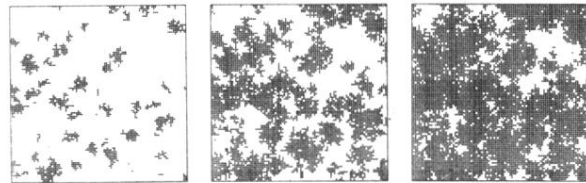


FIG. 3. Filling with Eden rates for $\alpha = 499$: typical occupied site distributions for $p = 0.15$, 0.5 (near p_c), and 0.75 .

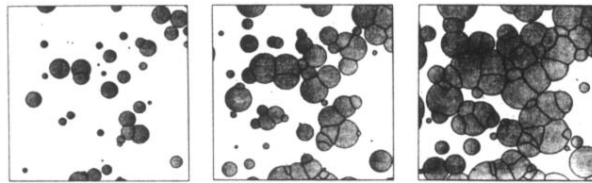


FIG. 4. Johnson-Mehl grain-growth patterns [provided by H. J. Frost, C. V. Thompson, and C. L. Howe (private communication)]. Circular grains nucleate at rate Γ , and expand radially at rate G . A fraction $p = 1 - \exp(-\pi\Gamma G^2 t^3/3)$ of the plane is converted at time t . Patterns shown for $p \approx 0.2, 0.53$, and 0.84 also indicate the curves along which grains first met.

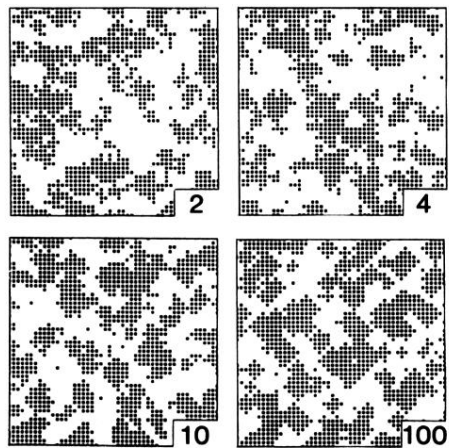


FIG. 9. Typical occupied site distributions, at $p = \frac{1}{2}$, for filling with $\alpha = 49$ Eden rates, and multiple-hit (M) noise reduction. Various M values are shown.